Advanced Fiber Materials (2024) 6:852–864
https://doi.org/10.1007/s42765-024-00383-y

RESEARCH ARTICLE

Pre-oxidized PAN Nanofibrous Membrane to Efficiently and Continuously Separate Large-Scale Viscous Oil-in-Water Emulsions Under Harsh Conditions with Ultra-Long-Term Oil-Fouling Recovery

Hongwei Su[1,2] · Hua Hu[3] · Zhenyu Li[1,2] · Guilong Yan[1,2] · Li Wang[1,2] · Dong Xiang[1,2] · Chunxia Zhao[1,2] · Yuanpeng Wu[1,2] · Jingyu Chen[1,2] · Ce Wang[4]

Received: 10 October 2023 / Accepted: 23 January 2024 / Published online: 26 March 2024

Abstract

High-performance multifunctional filtration membranes are highly required in treating practically complex oily wastewater systems, but still a challenge unsolved. Herein, we propose a facile route to address these challenges simultaneously by simply constructing electrospun pre-oxidized polyacrylonitrile nanofibrous membrane (p-PAN NM). Given the pre-oxidation process, the p-PAN NM displays not only robust anti-corrosive tolerance against diverse corrosive media, but also superhydrophilicity/underwater superoleophobicity. Additionally, ~ 99% separation efficiency, ~ 100% oil-fouling recovery, and ultra-long service life (up to 265 h) have been realized in separating large-scale surfactant stabilized soybean/crude oil-in-water emulsions. Furthermore, strong anti-corrosive performance against various corrosive media (e.g., 1 M HCl, 1 M NaOH, or 10 wt% NaCl) has been achieved as well. Spin-unrestricted density functional theory (DFT) computations implemented in the Dmol3 modulus has been conducted to understand the robust fouling recovery and the variation of surficial wettability after pre-oxidation. These outstanding filtration functions make our NM hold great potential in separating viscous oil/water emulsions under harsh conditions.

Keywords Pre-oxidized PAN · Anti-harsh conditions · Viscous oil-in-water emulsions · Emulsions separation · Fouling recovery

✉ Zhenyu Li
zhenyu.li@swpu.edu.cn

✉ Guilong Yan
guilong.yan@swpu.edu.cn

✉ Jingyu Chen
jingyu.chen@swpu.edu.cn

✉ Ce Wang
cwang@jlu.edu.cn

[1] The Center of Functional Materials for Working Fluids of Oil and Gas Field, School of New Energy and Materials, Southwest Petroleum University, Chengdu 610500, China

[2] Sichuan Engineering Technology Research Center of Basalt Fiber Composites Development and Application, State Key Laboratory of Oil and Gas Reservoir Geology and Exploitation, Southwest Petroleum University, Chengdu 610500, China

[3] PetroChina Southwest Oil and Gas Field Company Exploration Division, Chengdu 610500, China

[4] Alan G. MacDiarmid Institute, College of Chemistry, Jilin University, Changchun 130012, China

Introduction

During the past several decades, oily pollution, originated from oil spillage, domestic lives, and industrial activities, have caused huge threats to current ecological systems [1, 2]. Thus many methods for oily wastewater purification have been developed such as skims, air flotations, adsorbents, chemical or biological treatments, and filtration membrane (FM) [3, 4]. Among these methods, FM-based purification technique has gained special attention for their low cost, high separation efficiency, and less energy consumption [5–12].

For the lower viscosity of water than these of oils, FMs with superhydrophilicity/underwater superoleophobicity have been widely investigated in oil-in-water (O/W) emulsion purification. The absorbed water layer on the surface of FMs could effectively reduce the direct contact between oil droplets and the surface of FMs, lowering the risk of oil fouling. [13–17]. Li fabricated superhydrophilic FM by decorating MXene on electrospun polylactide NM. The rejection efficiency of the as-prepared FM against different O/W

emulsions was up to 99% [18]. Guzman and co-workers reported polydopamine-sulfobetaine methacrylate nanoparticles/cellulose acetate composite membrane for oil–water separation. The separation efficiency against different oil-in-water emulsions ranged from 95 to 99% [19]. Although many successes have been realized, the oil-fouling issues for long-term O/W emulsions treatment are still inevitable, in which some small-sized oil droplets could penetrate into the inner voids of NMs or adhere to the surface of NM, reducing the filtration efficiency [20–24]. To solve this bottleneck problem, many routes have been explored. Jiang and co-workers reported a double-defensed membrane by grafting poly(sulfobetaine) brushes onto poly(hydroxyethyl methylacrylate) hydrogel modified poly(vinylidene fluoride) porous membrane [25]. The membrane could continuously separate different surfactant-stabilized O/W emulsions for 6 h with the unchanged flux. Jin and co-workers fabricated zwitterionic nanosized hydrogels grafted poly(vinylidene fluoride) porous membrane [26]. The membrane could separate Tween80-stabilized isooctane-in-water emulsion for 10 h with 99% recovery of flux. Although many successes have been obtained, most literatures focus on the surfactant-stabilized non-viscous O/W emulsions separation.

Another factor, hindering the practical application of FMs in oily wastewater emulsion separation, originates from the threats of corrosive media (e.g. HCl, NaOH, and NaCl solution) [27–31]. To solve this problem, many efforts have been carried on to enhance the harsh conditions tolerance of FMs [32–37]. For example, Zhan et al. used engineering poly(phenyl-propionic nitrile) (PEN) to construct ternary PEN/halloysite nanotubes/graphene oxide FM. Even under harsh conditions including high-temperature resistance (up to 90 °C) and corrosive media (pH = 1 and pH = 14), the separation efficiency of as-prepared FM for O/W emulsions was still higher than 99% [33]. Wu and Chen constructed hydrophilic nanofibrous membrane (NM) with poly(*N*-isopropylacrylamide-*co*–*N*-methylolacrylamide) nanofiber as matrix and chitin nano-whisker as reinforcement via co-crosslinking route. The NM possessed high separation efficiency of > 99.5% with good flux of 1, 100–1, 300 L m^{-2} h^{-1} against Tween 80-stablized O/W emulsions under broaden pH values (pH = 1–13) [38]. Although many successes have been realized, the FMs, with both high anti-corrosive performance and ultra-long-term oil-fouling recovery for large-scale surfactant-stabilized viscous O/W emulsion separation are still highly required.

Herein, we proposed an alternative route to solve these two challenges above by constructing pre-oxidized polyacrylonitrile (p-PAN) NM. Given the cyclization, dehydrogenation, and oxidation within pre-oxidation, both the conjugated ladder molecular structures and the hydrophilic groups formed throughout the p-PAN [39–45]. The former provided p-PAN NM with high robust anti-corrosive capacity and high mechanical performance, the latter enabled the NM with superhydrophilic/underwater superoleophobic wettability. Consequently, our NM could continuously separate surfactant-free/surfactant-stabilized viscous (soybean oil or crude oil) O/W emulsions under harsh conditions (e.g., 1 M HCl, 10 wt% NaCl, 1 M NaOH) for 265 h with both high separation efficiency and robust oil-fouling recovery. What is more, robust stability against some organic corrosive media (e.g. N, N-dimethyl formamide (DMF), dimethylacetamide (DMAC), formic acid (FA), or dimethyl sulfoxide (DMSO)) has been also realized.

Experimental Section

Materials

Polyacrylonitrile (PAN) with an average molecular weight of about 150, 000, ethanol, N,N-dimethylformamide (DMF: ≥ 99.8%), dimethyl sulfoxide (DMSO: ≥ 99.9%), formic acid (FA: ≥ 96%), and dimethylacetamide (DMAC: ≥ 99.8%) were purchased from Sigma-Aldrich (Shanghai, China) Trading Co., Ltd. Diesel, soybean oil, HCl, NaOH, NaCl, and sodium dodecyl sulfonate (SDS) were provided by Kelong Chemical Co., Ltd. (Chengdu, China). Ampliflu Red and Ocean Blue were purchased from Aladdin Chemistry Co., Ltd. (Shanghai, China). The crude oil was provided by Daqing Oilfield and diluted with diesel fuel.

Preparation of Electrospun PAN Nanofibrous Membrane

1 g of PAN was added to 10 mL DMF, and the solution was heated under magnetic stirring at 70 °C for 12 h. PAN NM was fabricated through electrospinning, with the temperature, feed rate, applied voltage, and distance between the spinneret and collector fixed at 25 ± 2 ℃, 1 mL/h, 18 kV, and 20 cm, respectively.

Pre-oxidation Process

The PAN NM was placed in an oven and heated from 40 to 238 ℃, then to 248 ℃, and finally to 260 ℃ in air. Each stage was dwelled for 30 min with the heating rate of 5 ℃/min.

Preparation of Oil-in-Water Emulsion

Surfactant-free oil-in-water emulsions were achieved by mixing oil into deionized water (DI water) (V_{oil}:V_{water} = 1:99) under magnetic stirring (1, 200 rpm) for 30 min. Then, the mixture was sonicated (output power: 550 W) for 3 h to form a milk-like emulsion. As for surfactant-stabilized

oil-in-water emulsions, SDS was chosen as the emulsifier and dissolved into the aforementioned oil/water system. The concentration of SDS was fixed at 0.1 g/L within the final emulsions.

Separation of Oil-in-Water Emulsion

Two routes have been used for emulsions separation.

(i) *As for small amount oil-in-water emulsions separation:* The separation test was performed using a dead-end equipment setup, where the pre-wetted p-PAN nanofiber membrane, with the filtration area of 2.01 cm^2, was secured between the glass tube and the filter sand core. 20 mL of emulsions were added to the glass tube for filtration under a pressure of 0.09 MPa.

(ii) *As for large-scale viscous oil-in water emulsions separation:* The separation test was performed using a homemade setup, in which the p-PAN nanofiber membrane, with a stainless-steel mesh as a substrate, was fixed to a glass tube (with an area of 2.06 cm^2) using hydrophilic tape as a binder. The entire glass tube was immersed in a 2 L beaker containing 1.1 L of surfactant-free/surfactant-stabilized viscous oil-in-water emulsion, which was stirred magnetically at 400 rpm to simulate a flow oily wastewater system. Two filter flasks (2.5 L each) were connected between the glass tube and the water pump. One flask was used to collect the filtrate, while the other flask, acting as a buffer flask, was used to prevent backflow from the water pump. The entire filtration process was conducted under a pressure of 0.09 MPa.

Filtration function: The water flux J (L m^{-2} h^{-1} bar^{-1}) could be calculated by using Eq. (1) [46]:

$$J = \frac{V}{A \times t}, \tag{1}$$

where V (L) is the permeation volume of filtrate permeated through the membrane, t (h) is the filtration time, A (m^2) is the useable filtration area.

The filter efficiency R (%) is defined as Eq. (2)

$$R(\%) = \left(1 - \frac{C_f}{C_p}\right), \tag{2}$$

where C_p is the concentration of prepared solution and C_f is the concentration of the filtrate solution. As for large-scale viscous O/W emulsion separation, we recorded the time per 50 mL O/W emulsion separation. Thus, the flux versus time (volume) can be calculated.

Anti-fouling Assessment

To clearly demonstrate the anti-fouling performance, the viscous oil droplets were dyed with Ampliflu Red. After filtration, the fouled nanofiber membrane (NM) was placed in an 80 ℃ water bath and subjected to ultrasonic treatment for 5 min to remove the fouled oil droplets. Ultraviolet (UV) lamp was used to illuminate both the fouled membrane and the recovered membrane.

DFT Calculation Details

All simulation and calculation experiments were carried out under the Materials Studio. The generalized gradient approximation of Perdew–Burke–Ernzerh (PBE) was used in Dmol3 modulus with OTFG ultra-soft pseudopotential. The kinetic energy cutoffs were all set to 480 eV, and the Brillouin zone was sampled with a special Monkorst-park K-point grid of $4 \times 4 \times 1$ for geometry optimization and energy task. The SCF tolerance, maximum force, maximum stress and maximum displacement were all set as 2.0×10^{-5} eV/atom, 0.05 eV/ Å, 0.1 GPa and 0.001 Å, respectively.

Characterizations

A field-emission scanning electron microscope (Thermo Scientific Apreo 2 C, USA) was utilized for SEM analysis. Atomic force microscope (AFM) was used for roughness analysis using a BRUKER Dimension ICON, (Germany). The chemical composition of the nanofibrous membrane surface was fully characterized using Fourier transform infrared (FTIR) spectra obtained from a Bruker Lumos FT-IR Microscope (Billerica, MA, USA) in ATR mode. X-ray photoelectron spectroscopy (XPS) was conducted using a Thermo Fisher Escalab 250 Xi instrument (Waltham, MA, USA), with Al Kα as the excitation source. Contact angles (CAs) were measured using an OCA 25 data physics contact angle meter (Germany). Mechanical properties test was performed using a universal testing machine (UTM, CS 225, Lloyd Instruments, Ltd., UK). The average total organic carbon (TOC) content in the feed solutions and corresponding filtrates was determined using a Shimadzu TOC-L total organic carbon analyzer (Japan). Optical images were captured using a Canon EOS 50 D camera (Tokyo, Japan). Dynamic light scattering (DLS) characterization was performed using a Zetasizer instrument (Nano-ZS, Malvern, UK).

Results and Discussion

Synthesis and Characterization of p-PAN NM

Figure 1 illustrates the whole synthetic procedures for p-PAN NM. Briefly, PAN NM was obtained by electrospinning PAN/DMF solution. Pre-oxidation was then employed to treat the PAN NM, in which cyclization, dehydrogenation, and oxidation occurred simultaneously [47, 48], resulting in the formation of conjugated ladder molecular structures and hydrophilic groups throughout the p-PAN NM. Besides, the roughness of p-PAN NM was smaller than that of PAN NM (ESI; Fig. S1), attributing to the stretching of the membrane during pre-oxidation process. Thus, p-PAN NM with strong anti-corrosion properties, good mechanical performance, and superhydrophilicity/underwater superoleophobicity was fabricated for highly efficient oil/water emulsion separation.

To confirm the reactions during the pre-oxidation process, Fourier transform infrared spectra (FTIR) with ATR model and X-ray photoelectron spectra (XPS) were combined to characterize the PAN and p-PAN NM. From the FTIR spectra (Fig. 2a), PAN NM exhibited two peaks (2, 941 cm^{-1} and 1, 452 cm^{-1}) corresponding to C-H stretching bonds, as well as a peak (2, 243 cm^{-1}) for the C≡N vibrating band [49]. After pre-oxidation, the relative intensities of both the C≡N vibrating bands (2,243 cm^{-1}) and the C-H vibrating bonds (2,941 cm^{-1}) decreased. Simultaneously, a new and strong band emerged at 1,596 cm^{-1}, indicating the formation of C=N vibrating bands. Additionally, a new peak at 807 cm^{-1}, associated with (C = C in the aromatic rings), was also observed [50] confirming the cyclization and dehydrogenation reactions. Furthermore, two weak peaks at 1, 725 cm^{-1} and 1, 252 cm^{-1}, corresponding to the C=O and C–O groups, respectively, were detected. The broadened peak around 3, 235 cm^{-1}, indexing to the OH group, confirmed the oxidation reaction.

Figure 2b displays the XPS survey spectra of PAN NM and p-PAN NM, revealing the appearance of strong O 1 s peaks after pre-oxidation. Figure 2c presents the high-resolution spectrum of C 1 s from PAN NM, showing two peaks at 284.8 and 283.5 eV for C≡N and C–C/C–H, respectively [51]. In the case of p-PAN NM, the C 1 s peak can be deconvoluted into four peaks when considering the elements and groups directly bonded to the carbon atoms (Fig. 2d) [52]. The N 1 s spectrum of p-PAN NM exhibited a new peak at around 399.9 eV, indicating aromatic C=N was formed during peroxidation (Fig. 2e) [53]. The O 1 s peak of p-PAN NMs was deconvoluted into two peaks at 531.4 and 533.1 eV, corresponding to C–O and C=O, respectively (Fig. 2f) [54].

Variation of Surficial Wettability and Theoretical Elucidation

The variation of PAN NM surficial wettability before and after pre-oxidation has been systematically investigated. To vividly demonstrate the wettabilityNM with the aid of a UV lamp, indicating the hydrophobicity/lipophilicity of PAN NM and the amphiphilicity of p-PAN NM in air. Figure 3c illustr, Fig. 3a, b presents the photos of water and oil droplets on PAN and p-PAN NM. For PAN NM, water droplets remained on the surface while oil droplets (1, 2-dichloroethane was used) penetrated into the NM. In contrast, both water (dyed with Ocean Blue) and oil droplets (dyed with Ampliflu Red) quickly penetrated the p-PAN ates the water and oil contact angles (WCA and OCA) of PAN NM were 135° and 0°, respectively. The underwater oil contact angle (UWOCA) and underoil water contact angle (UOWCA) were 126° and 145°, respectively. For p-PAN NM (Fig. 3d), the WCA, OCA, UWOCA, and UOWCA were 0°, 0°, 156°, and 150°, respectively, confirming the superamphiphilicity in air, underwater superoleophobicity, and underoil superhydrophobicity of p-PAN NM. UWOCAs of different oil droplets (1, 2-dichloroethane, chloroform, diesel, crude

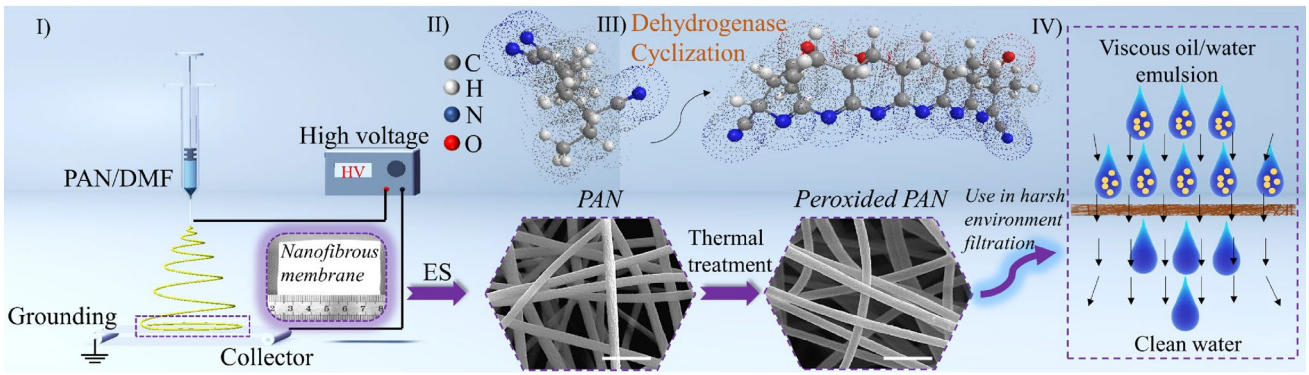

Fig. 1 Schematic diagrams for the preparation of p-PAN NM and its application in oil/water emulsion separation

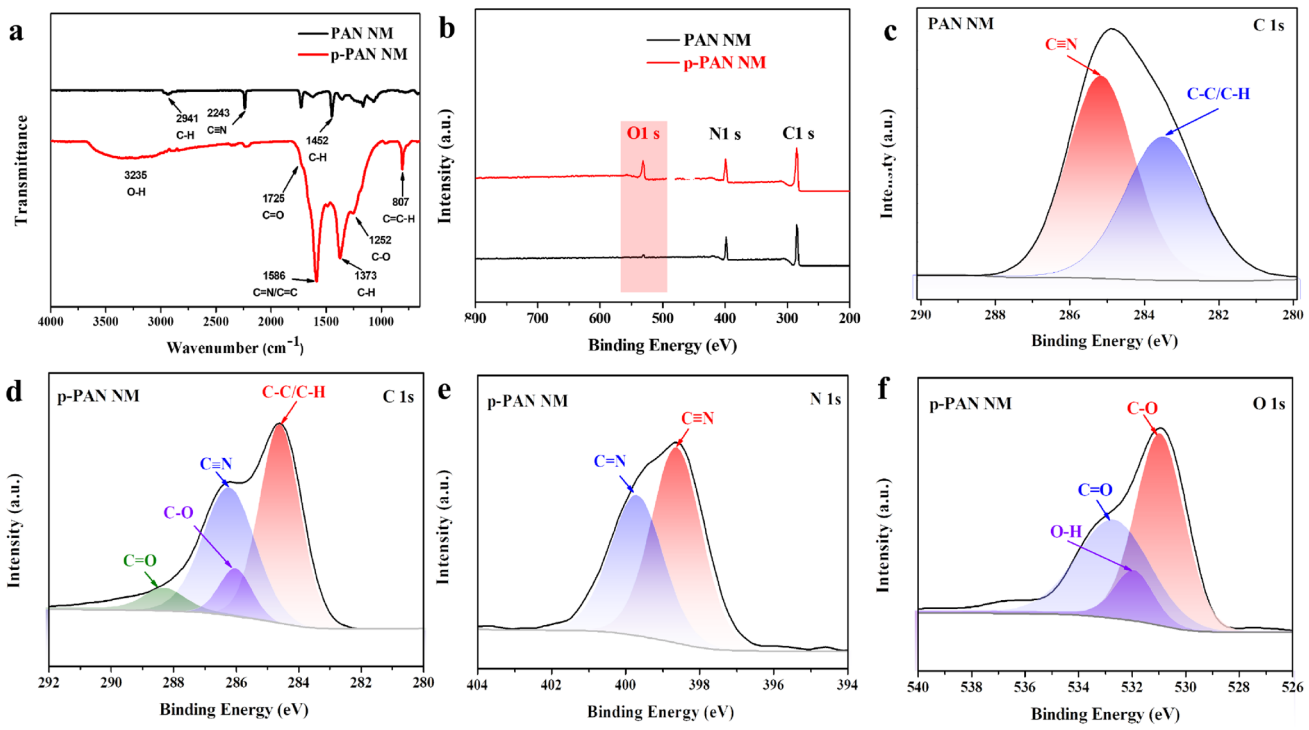

Fig. 2 **a** FITR-ATR spectra and **b** XPS survey spectra of PAN and p-PAN NM. **c** C 1 s high-resolution of PAN NM. **d-f** C 1 s, N 1 s, and O 1 s high-resolution of p-PAN NM, respectively

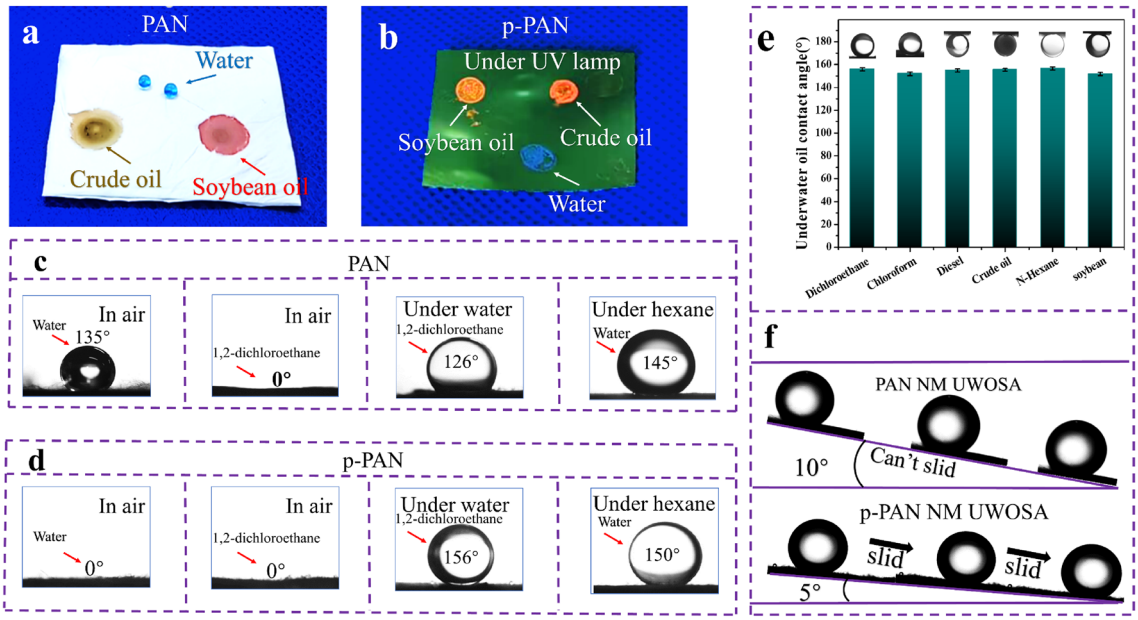

Fig. 3 **a** and **b** Photos of water and oil droplets on PAN and p-PAN NM. **c** and **d** WCA, OCA, UWOCA, and UOWCA of PAN and p-PAN NM. **e** UWOCAs of p-PAN NM against different oil droplets. **f** UWOSA of PAN and PAN NM

oil, N-hexane, and soybean) have been measured (Fig. 3e), proving the generality of underwater superoleophobicity of p-PAN NM. The underwater oil adhesion on PAN NM and p-PAN NM was also investigated by measuring the underwater oil sliding angle (UWOSA). Even PAN NM was tilted to 10°, the oil droplet still tightly adhered to the NM (Top of

Fig. 3f). In contrast, p-PAN NM (Bottom of Fig. 3f) exhibited a lower UWOSA (~5°), indicating the reduced oil adhesion of p-PAN NM.

To clearly understand the variation of surficial wettability, all spin-unrestricted density functional theory (DFT) computations were implemented using the Dmol3 code. Electron exchange and correlation effects were evaluated using the Perdew-Burke-Ernzerhof (PBE) generalizing gradient approximation (GGA). The optimized adsorption structures of H_2O and oils (*It is important to note that three representative oils (cyclohexane, 1, 2-dichloroethane, and chloroform) with well-defined structures were chosen as models to replace the traditional viscous oils (soybean oil or crude oil) owning to their not defined structures*) on the surface of PAN and p-PAN were studied. The adsorption energy (Ea) of PAN and p-PAN for both water and oils was calculated at 25 ℃. From Fig. 4a, it could be observed that the Ea of PAN for water was positive, indicating the hydrophobicity (as proven in Fig. 3c). In contrast, the Ea values of PAN for oils were all negative, confirming the lipophilicity. For p-PAN NM (Fig. 4b), all Ea values were negative, demonstrating the super-amphiphilicity of p-PAN NM in air environment (as observed in Fig. 3d).

Measurement of Anti-harsh Conditions Tolerance

Strong tolerance to harsh conditions is of great importance for effectively separating oily wastewater systems coupled with corrosive media [55–59]. To evaluate the tolerance of our p-PAN NM against various normal inorganic solutions (e.g., 100 ℃ boiling water, 1 M HCl, 1 M NaOH, 10 wt% NaCl, and DI Water) and strong corrosive organic solvents (DMF, DMAC, DMSO, and FA) at room temperature (25 ± 2 ℃) was measured by immersing the NM in these media for 7 days (Fig. 5a and b). Additionally, the stability of p-PAN NM under ultrasonic treatment in an 80 ℃ hot water bath for 1 h was also tested (ESI, Fig. S2). From these data, we could observe that our NM maintained its integrity and the media remained transparent, implying no reactions occurred between our NM and the media. To further validate our

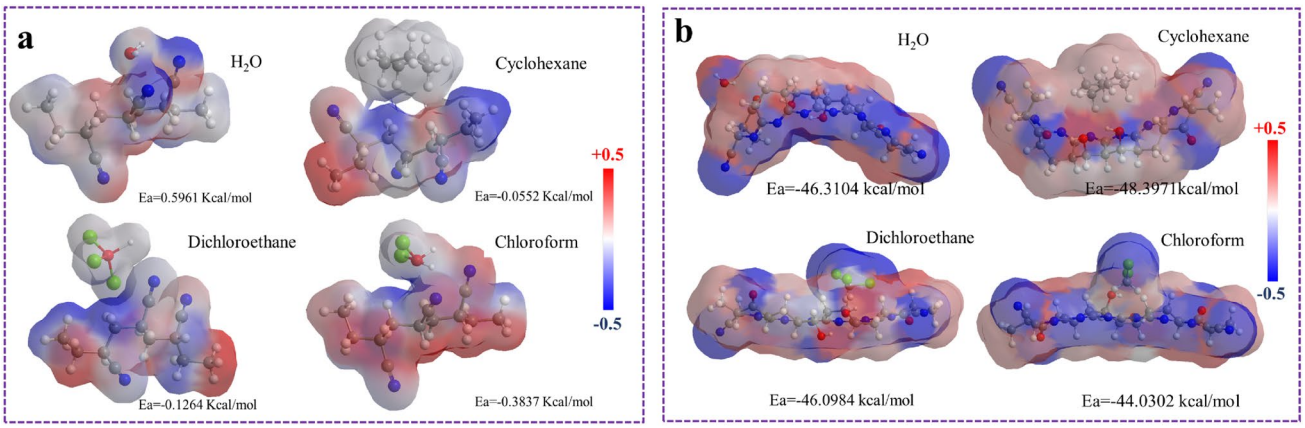

Fig. 4 Electrostatic potential diagrams on Ea of the water, cyclohexane, 1, 2-dichloroethane, and chloroform on **a** PAN NM and **b** p-PAN NM at 25 ℃, respectively

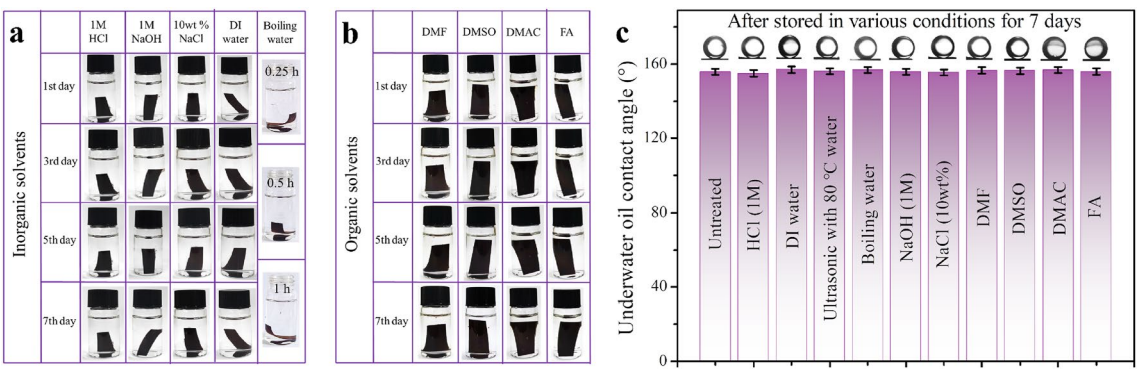

Fig. 5 Photographs of p-PAN NM stored within **a** inorganic solvents, **b** organic solvents, respectively. **c** Underwater oil contact angles of p-PAN NM after being treated under harsh conditions

hypothesis, the surficial wettability of p-PAN NM before and after these treatments was evaluated by measuring the UWOCA with 1, 2-dichloromethane as model (Fig. 5c). These unchanged UWOCA indicated that the surficial wettability of p-PAN NM was not affected. In contrast, PAN NM exhibited instability when exposed to these media (ESI, Fig. S3). PAN NM became curled when contacting with the inorganic media and organic FA solvent. As for organic solvents (DMF, DMSO, and DMAC), PAN NM dissolved completely within 1 s. The mechanical properties of PAN NM and p-PAN NM have been measured (ESI, Fig. S4). Given the cyclization reaction within pre-oxidation process, the tensile stress of p-PAN was higher than that of PAN NM.

O/W Emulsion Separation Performance

To evaluate the efficiency of separating oil-in-water (O/W) emulsions, a series of O/W emulsions, including both SDS-free and SDS-stabilized emulsions, were prepared and filtered via p-PAN NM. Optical microscopy and digital imaging were employed to visually track the changes in the feeds and filtrates with SDS-free/SDS-stabilized cyclohexane-in-water emulsions as model system (Fig. 6a, b). It was observed that all the creamy feeds turned transparent and the oil droplets completely disappeared after filtration. The size distribution variations of the O/W emulsions in the feeds and filtrates were measured using dynamic light scattering (DLS) (ESI; Fig. S5). The effectiveness of this high separation efficiency against different types of O/W emulsions was evaluated by filtering eight different SDS-free/SDS-stabilized O/W emulsions (containing dichloroethane, cyclohexane, soybean oil, and crude oil) using p-PAN NM (Fig. 6c). All the separation efficiencies were found to exceed 99.7%. Figure 6d illustrates the cycling stability of SDS-free cyclohexane-in-water emulsions for ten cycles. It can be observed that both the flux and separation efficiency remained constant over the course of ten cycles, demonstrating the excellent cycling stability of our p-PAN NM.

Long-Term Separation of SDS-Free/SDS-Stabilized Liter-Scale Soybean/Crude O/W Emulsions Under Harsh Conditions

To assess the separation efficiency of our p-PAN NM for large-scale viscous O/W emulsion separation, we employed a home-made filtration device (ESI; Fig. S6). A beaker containing 1.1 L of viscous O/W emulsion was subjected to moderate magnetic stirring (300 rpm) to simulate the existing O/W emulsions in a flowing aquatic system. The left flask collected the filtrate while the right one prevented sucking-back. The entire setup was driven by a water pump. Data in Fig. 7a, b indicated that both liter-scale creamy SDS-free soybean and crude O/W emulsions (feed) turned transparent after filtration (filtrate). The size distribution variations of the viscous O/W emulsions in the feeds and filtrates were measured using dynamic light scattering (DLS) (ESI; Fig. S7). To evaluate the long-term separation efficiency and cycling stability, Fig. 7c, d depicts the

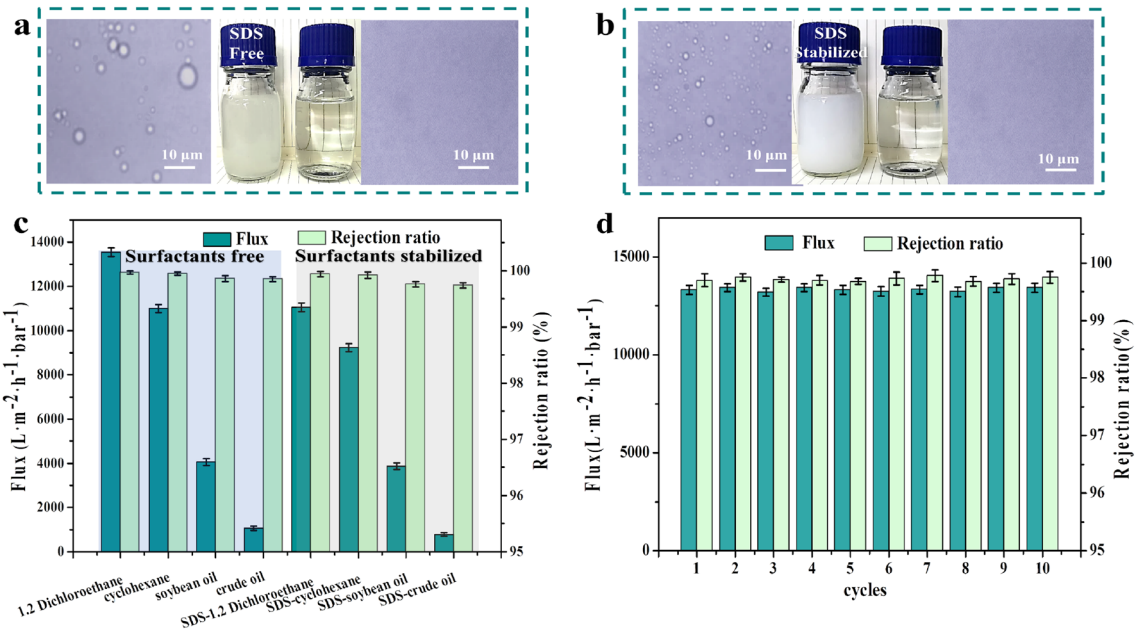

Fig. 6 The optical microscope and digital images for feeds and filtrates of **a** surfactant free and **b** surfactant stabilized O/W emulsions. **c** Separation efficiencies and fluxes for different emulsions. **d** Cycling stability for cyclohexane O/W emulsion for ten times

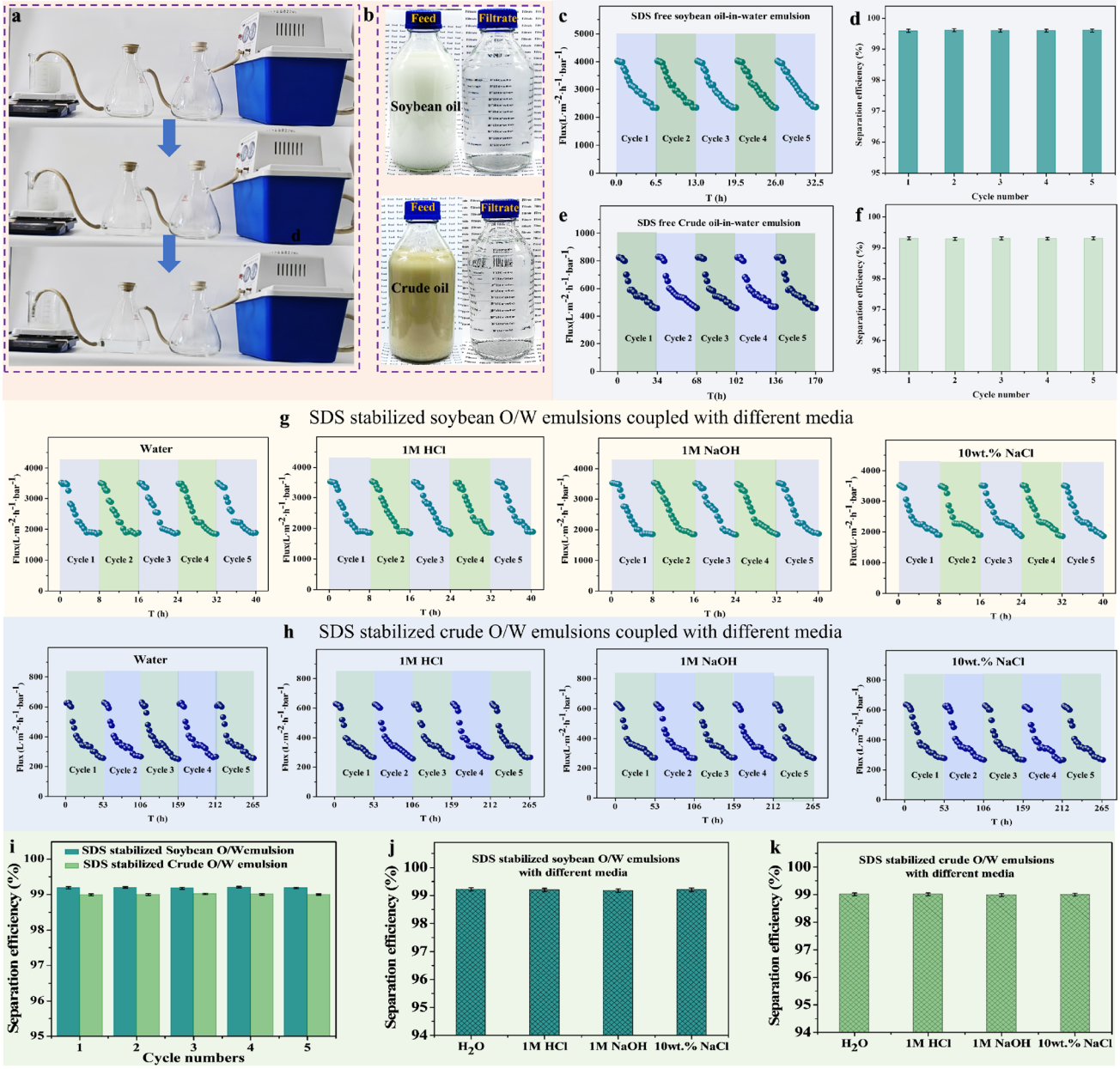

Fig. 7 **a** Digital photos of the process of liter-scale viscous O/W emulsions separation. **b** Photographs of the feed and filtrate of SDS-free soybean/crude O/W emulsions before and after separation. **c** and **d** are the variation of flux versus time of SDS-free soybean/crude O/W emulsions separation for 5 cycles, respectively. **e** and **f** the variation of separation efficiency for SDS-free soybean/crude O/W emulsions separation for 5 cycles, respectively. **g** and **h** are SDS-stabilized soybean and crude O/W emulsions separations coupled with different media for 5 cycles. **i** is the separation efficiency of these two SDS-stabilized O/W emulsions for 5 cycles. **j** and **k** are separation efficiency of these two SDS-stabilized O/W emulsions coupled with different media

variation in permeating flux versus time during five cycles of separation. From the curves, it can be observed that the permeating flux of both SDS-free O/W emulsions could be completely recovered, achieving 100% flux recovery ratio (FRR) (Fig. 7e and f) for 170 h of continuous separation.

The components present in real oil-contaminated effluents, generated from industrial processes and daily activities, are rather complex. Various pollutants, including acids, alkalis, salts, and surfactants, often coexist with oil droplets. To evaluate the purification capacity of p-PAN NM under harsh conditions for real oil-contaminated effluents, we conducted long-term continuous separation experiments using liter-scale SDS-stabilized soybean O/W and crude O/W emulsions in the presence of corrosive media. Figure 7g illustrates the long-term cycling performance of p-PAN NM for SDS-stabilized soybean O/W emulsion coupled with

H_2O, 1 M HCl, 1 M NaOH, or 10 wt% NaCl over five cycles. From these curves, it can be observed that our p-PAN NM exhibits excellent recycling stability. Even when the separation time reached *265* h (Fig. 7h) for SDS-stabilized crude O/W emulsion coupled with H_2O, 1 M HCl, 1 M NaOH, and 10 wt% NaCl over five cycles, a 100% FRR was achieved, demonstrating the robustness and ultra-long-term cycling stability of p-PAN NM under harsh conditions. Figure 7i, j, and k clearly demonstrates the maintained high separation efficiency (≥ 99.0% for crude O/W emulsions and 99.2% for soybean O/W emulsion), regardless of the corrosive media. *This exceptional ultra-long-term continuous separation*

Table 1 Comparison of separation efficiency (SE), continuous separation time (CST), separated targets (ST), FRR, and harsh conditions Testing (HCT) in similar literatures and our work

Materials	SE (%)	CST (h)	STs		FRR (%)	HCT	Refs.
			Type of emulsion	Separation Volume (L)			
ZNG-g-PVD membrane	99.8%	10 h	Tween80-stabilized non-viscous isooctane-in-water emulsion	1.5	~ 100%	Not provided	[26]
$Bi_2MoO_6/Cu_3(PO_4)_2$ nanosheet-coated copper mesh	> 97.2%	5 h	CTAB-stabilized non-viscous cyclohexane-in-water emulsion	0.5	~ 100%	Not provided	[60]
pSB brushes grafted PVDF @ pHEMA membrane	99.1%	6 h	Tween 80-stabilized hexadecane-in-water emulsion	0.4	~ 100%	Not provided	[25]
ZIF-8/hydrolyzed PAN NM	99%	42 h	SDS stabilized dodecane-in-water emulsion	10	~ 98.5%	Not provided	[61]
PPy decorated poly(vinyl alcohol) NM	99%	7 h	SDS stabilized pump oil-in-water emulsion	Not provided	~ 97.5%	Yes	[62]
epigallocatechin gallate/Ag decorated PVDF membrane	95%	70 min	SDS-stabilized diesel-in-water emulsion	Not provided	98.1%	Yes	[63]
perfluorohexanoic acid modified Poly(phenylene sulfide) membrane	> 98%	3.5 h	Hexadecane-in-water emulsion	Not provided	> 85%	Yes	[64]
TA/AEPPS modified acid @pPVDF/PHEMA membrane	99.2%	2.5 h	Crude oil-in-water emulsion	Not provided	94.1%	Yes	[65]
PVDF/PDH Membrane	99%	12 h	Isooctane-in-water emulsion	Not provided	91%	Not provided	[66]
SPAN-PPy/ZnO NFMs	> 96.1%	Not provided	SDS stabilized petroleum-in-water emulsion	0.2	96%	Not provided	[67]
SPAN/β-FeOOH NM	> 98.2%	Not provided	SDS stabilized petroleum-in-water emulsion	0.1	Not provided	Yes	[68]
Pre-oxidized PAN NM	99.2%	40 h[a]	SDS-stabilized soybean oil-in-water emulsion	5	100%	Yes	This work
	99%	265 h[b]	SDS-stabilized crude oil-in-water emulsion	5	100%	Yes	

ZNG-g-PVDF zwitterionic nanosized hydrogels grafted poly (vinylidene fluoride), *D5* Decamethylcyclopentasiloxane, *pSB* poly(sulfobetaine), *PVDF* poly(vinylidene fluoride), *pHEMA* poly(hydroxyethyl methylacrylate) membrane, *ZIF-8* Zeolitic imidazole framework-8, *TA* tannic acid, *AEPPS* N-aminoethyl piperazine propane sulfonate, *PHEMA* poly(2-hydroxyethyl methacrylate), *PDH* poly(dimethylaminoethyl methacrylate-co-2-hydroxyethyl methacrylate), *PPy* polypyrrole, *SPAN* stabilized polyacrylonitrile, *Pre-oxidized PAN NM* polyacrylonitrile nanofibrous membrane

[a]The pre-oxidized PAN NM could continuously separate SDS-stabilized soybean oil-in-water emulsion for 40 h under harsh conditions with 100% flux recovery ratio

[b]The pre-oxidized PAN NM could continuously separate SDS-stabilized crude oil-in-water emulsion for 265 h under harsh conditions with 100% flux recovery ratio

capacity for surfactant-stabilized viscous O/W emulsions under harsh conditions surpasses most of the reported literature. To highlight the advantages of this work, Table 1 provides a comparison of separation efficiency, continuous separation time, targets, FRR, and harsh conditions with similar literature.

Fouling-Recovery/Theoretical Clarification and Mechanism of Separating O/W Emulsions

To vividly demonstrate the fouling recovery through ultrasound treatment in an 80 ℃ hot water bath, we utilized Ampliflu Red dyed SDS-stabilized soybean and crude O/W emulsions. Upon separation, it was observed that the surface of fouled p-PAN NM was completely covered by viscous oil cakes, which were clearly visible under a UV lamp. However, after subjecting the p-PAN NM to sonication treatment, these cakes disappeared entirely (Fig. 8a). Figure 8b displays the activation energy (Ea) values of p-PAN against water, cyclohexane/dichloroethane/chloroform vapors at 80 ℃. The data reveal an increased Ea value for water on p-PAN, indicating an enhanced affinity between water and p-PAN at 80 ℃. Conversely, the Ea values between p-PAN and these oil vapors decreased. Furthermore, the viscosity of viscous oil decreases at high temperature [69]. Considering the heightened affinity between water and p-PAN, reduced affinity between oils and p-PAN, decreased viscosity of viscous oil, as well as the vibrational fluid motion during ultrasound treatment [70], it can be inferred that these oil cakes on the surface or within the voids of p-PAN NM will be completely removed.

Figure 8c illustrates the emulsion separation mechanism of p-PAN NM. When water comes into contact with the surface of p-PAN NM in air, it diffuses and penetrates the membrane directly (left side of Fig. 8c), forming a stable water layer. According to Eq. (3), the porous surface of the water-covered p-PAN NM can withstand a certain intrusion pressure ($\Delta P > 0$) when submerged in water (right side of Fig. 8c), as the contact angle of oil droplets on the surface is greater than 90°.

$$\Delta P = \frac{2\gamma}{R} = -\frac{l\gamma(\cos\theta)}{A}, \tag{3}$$

where γ is the oil–water interfacial tension; R is the meniscus's radius; l is the circumference of the pore; A is the cross-sectional area of the pore; θ is the advancing contact angle of oil on the nanofiber surface. The water film on the surface of p-PAN NM creates underwater superoleophobicity and

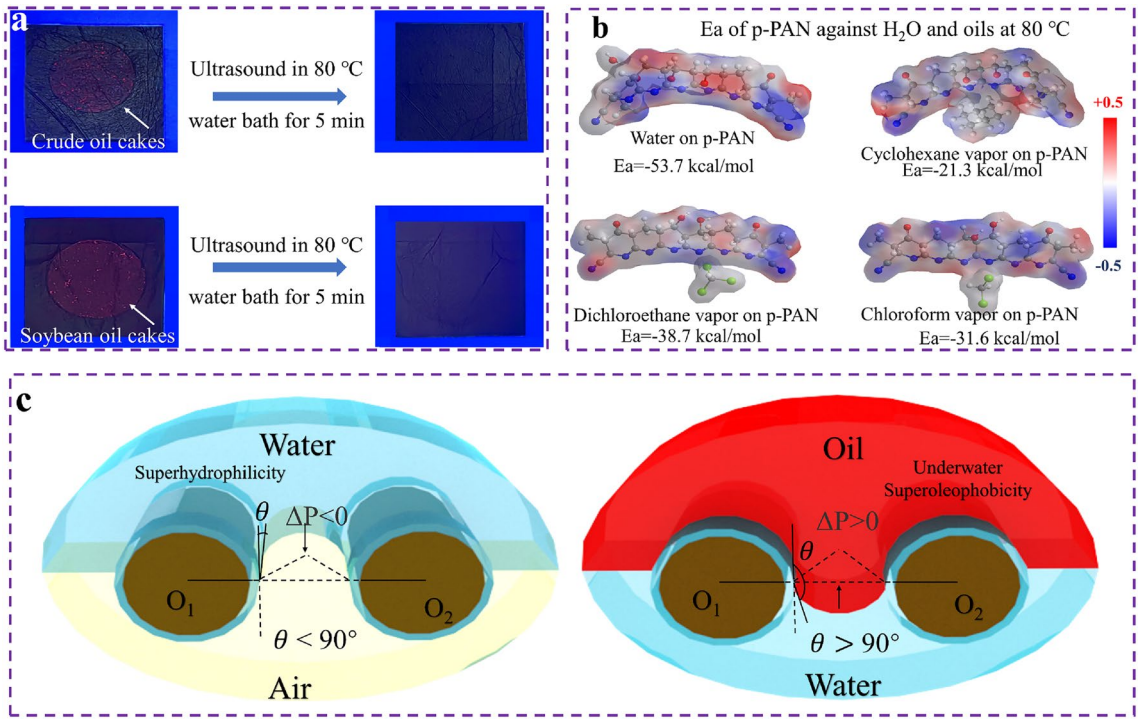

Fig. 8 a Photos on the surficial variations of viscous oil fouled NM before and after ultrasound. b Electrostatic potential diagram on Ea of the water, hexane, dichloroethane and chloroform absorbed on p-PAN NM at 80 °C. c Schematic diagram of the mechanism on separating O/W emulsions

oil-repellent properties. Throughout the separation process, the demulsified viscous oil droplets approach the NM surface and steadily accumulate due to transmembrane pressure, resulting in a reduction in permeating flux.

Conclusion

Electrospun pre-oxidized polyacrylonitrile (p-PAN) NM, with robust anti-corrosion, firm fouling recovery, and superhydrophilicity/underwater superoleophobicity has been prepared via one-pot Pre-oxidation process. Our p-PAN NM displayed high separation efficiency (~ 99%) and ~ 100% oil-fouling recovery for continuously (*265 h*) separating large-scale SDS-stabilized soybean/crude oil-in-water emulsions coupled with corrosive media. DFT computations have been adopted to clarify the robust fouling recovery and the variation of surficial wettability after Pre-oxidation. These outstanding filtration functions open a route for membrane filtration for durable and massive viscous oils/water emulsions separation under harsh conditions in practice.

Supplementary Information The online version contains supplementary material available at https://doi.org/10.1007/s42765-024-00383-y.

Acknowledgements This work was supported by the National Natural Science Foundation of China (No. 52073238 and 52173301), Open Funds of State Key Laboratory of Oil and Gas Reservoir Geology and Exploitation (PLN202205, SWPU), and Natural Science Foundation of Sichuan Province (2022NSFSC0356).

Funding National Natural Science Foundation of China, 52273055, Ce Wang, State Key Laboratory of Oil and Gas Reservoir Geology and Exploitation, PLN202205, Jingyu Chen, Sichuan Engineering Technology Research Center of Basalt Fiber Composites Development and Application, 2022SCXWYXWFC006, Jingyu Chen, Natural Science Foundation of Sichuan Province, 2022NSFSC0356, Jingyu Chen.

Data availability The data are available from the corresponding authors on reasonable request.

Declarations

Conflict of Interest The authors declare no conflicts of interest.

References

1. Al-Majed AA, Adebayo AR, Hossain ME. A sustainable approach to controlling oil spills. *J Environ Manage*. **2012**;*113C*:213.
2. Yin ZZ, Yuan F, Li M, Xue MS, Zhou DP, Chen YC, Liu XQ, Luo YD, Hong Z, Xie C, Ou JF. Self-cleaning, underwater writable, heat-insulated and photocatalytic cellulose membrane for high-efficient oil/water separation and removal of hazardous organic pollutants. *Pro Org Coat*. **2021**;*157*: 106311.
3. Xia Y, Zhang R, Cao Y, Xing Y, Gui X. Role of molecular simulation in understanding the mechanism of low-rank coal flotation: a review. *Fuel*. **2020**;*262*: 116535.
4. Yin ZZ, Li M, Li ZH, Deng YT, Xue MS, Chen YH, Ou JF, Lei S, Luo YD, Xie C. A harsh environment resistant robust $Co(OH)_2$@ stearic acid nanocellulose-based membrane for oil-water separation and wastewater purification. *J Environ Manage*. **2023**;*342*: 118127.
5. Wu JF, Cui ZW, Yu Y, Han H, Tian D, Hu JD, Qu JF, Cai YH, Luo JL, Li JZ. A 3D smart wood membrane with high flux and efficiency for separation of stabilized oil/water emulsions. *J Hazard Mater*. **2023**;*441*: 129900.
6. Liu KY, Yin ZZ, Luo RK, Qiu BR, Chen YH, Yang CG, Luo YD, Hong Z, Xue MS. Durable $Co(OH)_2$/stearic acid-based superhydrophobic/superoleophilic nanocellulose membrane for highly efficient oil/water separation and simultaneous removal of soluble dye. *Ind Crop Prod*. **2023**;*203*: 117190.
7. Yin ZZ, Li ZH, Deng YT, Xue MS, Chen YH, Ou JF, Xie Y, Luo YD, Xie C, Hong Z. Multifunctional CeO_2-coated pulp/cellulose nanofibers (CNFs) membrane for wastewater treatment: Effective oil/water separation, organic contaminants photodegradation, and anti-bioadhesion activity. *Ind Crop Prod*. **2023**;*197*: 116672.
8. Yin ZZ, Chen XX, Zhou TH, Xue MS, Li M, Liu KY, Zhou DP, Ou JF, Xie Y, Ren ZM, Luo YD, Hong Z. Mussel-inspired fabrication of superior superhydrophobic cellulose-based composite membrane for efficient oil emulsions separation, excellent antimicrobial property and simultaneous photocatalytic dye degradation. *Sep Purif Technol*. **2022**;*286*: 120504.
9. Yin ZZ, Cheng Y, Deng YT, Li ZH, Liu KY, Li M, Chen XX, Xue MS, Ou JF, Lei S, Luo YD, Xie C, Hong Z. Functional and versatile colorful superhydrophobic nanocellulose-based membrane with high durability, high-efficiency oil/water separation and oil spill cleanup. *Surf Coat Technol*. **2022**;*445*: 128714.
10. Long QW, Chen JX, Wang Z, Zhang Z, Qi GX, Liu ZQ. Vein-supported porous membranes with enhanced superhydrophilicity and mechanical strength for oil-water separation. *Sep Purif Technol*. **2021**;*254*: 117517.
11. Lu JQ, Bai T, Wang D, Yu HJ, Wang QX, Niu ZX, Hu Y, Liu XY, Han GP, Cheng WL. Electrospun polyacrylonitrile membrane in situ modified with cellulose nanocrystal anchoring TiO_2 for oily wastewater recovery. *Adv Fiber Mater*. **2023**;*5*:2055–68.
12. Zhao HD, He YL, Wang ZH, Zhao YB, Sun L. Mussel-inspired fabrication of PDA@PAN electrospun nanofibrous membrane for oil-in-water emulsion separation. *Nanomaterials*. **2021**;*11*:3434.
13. Jiang DH, Tsai PC, Kuo CC, Jhuang FC, Guo HC, Chen SP, Liao YC, Satoh T, Tung SH. Facile preparation of Cu/Ag core/shell electrospun nanofibers as highly stable and flexible transparent conductive electrodes for optoelectronic devices. *Acs Appl Mater Interfaces*. **2019**;*11*:10118.
14. Yan XH, Xiao X, Au C, Mathur S, Huang LJ, Wang YX, Zhang ZJ, Zhu ZJ, Kipper MJ, Tang JG, Chen J. Electrospinning nanofibers and nanomembranes for oil/water separation. *J Mater Chem A*. **2021**;*9*:21659.
15. Liu C, Ren QQ, Zhang SW, Yin BS, Que LF, Zhao L, Sui XL, Yu FD, Li XF, Gu DM, Wang ZB. High energy and power lithium-ion capacitors based on Mn_3O_4/3D-graphene as anode and activated polyaniline-derived carbon nanorods as cathode. *Chem Eng J*. **2019**;*370*:1485.
16. Liang LP, Dong YY, Wang HF, Meng X. Smart cotton fabric with CO_2-responsive wettability for controlled oil/water separation. *Adv Fiber Mater*. **2019**;*1*:222.
17. Oh S, Bang J, Jin HJ, Kwak HW. Green fabrication of underwater superoleophobic biopolymeric nanofibrous membranes for effective oil-water separation. *Adv Fiber Mater*. **2023**;*5*:603.

18. Chen SY, Deng YF, Huang T, Zhang N, Wang Y. Polydopamine-assisted MXene decoration on electrospun polylactide fibers toward oil/water separation and organic dye adsorption. *Sep Purif Technol*. **2024**;*328*: 125040.
19. Su Y, Fan TT, Cui WY, Li YA, Ramakrishna S, Long YZ. Advanced electrospun nanofibrous materials for efficient oil/water separation. *Adv Fiber Mater*. **2022**;*4*:938.
20. Tao LL. Bio-inspired anti-oil-fouling chitosan-coated mesh for oil/water separation suitable for broad pH range and hyper-saline environments. *Acs Appl Mater Interfaces*. **2013**;*5*:11971–6.
21. Sun A, Zhan YQ, Feng QY, Yang W, Dong HY, Liu YC, Chen XM, Chen YW. Assembly of MXene/ZnO heterojunction onto electrospun poly(arylene ether nitrile) fibrous membrane for favorable oil/water separation with high permeability and synergetic antifouling performance. *J Membr Sci*. **2022**;*663*: 120933.
22. Li BZ, Zhao J, Lin XX, Tu DG, Meng Y, Li YQ, Huang P, Zhang H. Highly efficient sunlight-driven self-cleaning electrospun nanofiber membrane NM88B@HPAN for water treatment. *J Clean Prod*. **2022**;*355*: 131812.
23. Chen XM, Zhan YQ, Sun A, Feng QY, Yang W, Dong HY, Chen YW, Zhang YJ. Anchoring the TiO_2@crumpled graphene oxide core-shell sphere onto electrospun polymer fibrous membrane for the fast separation of multi-component pollutant-oil-water emulsion. *Sep Purif Technol*. **2022**;*298*: 121605.
24. Ma WJ, Li YS, Zhang MJ, Gao ST, Cui JX, Huang CB, Fu GD. Biomimetic durable multifunctional self-cleaning nanofibrous membrane with outstanding oil/water separation, photodegradation of organic contaminants, and antibacterial performances. *Acs Appl Mater Interfaces*. **2020**;*12*:34999.
25. Dong D, Zhu Y, Fang W, Ji M, Wang A, Gao S, Lin H, Huang R, Jin J. Double-defense design of super-anti-fouling membranes for oil/water emulsion separation. *Adv Funct Mater*. **2022**;*32*:2113247.
26. Zhu Y, Wang J, Zhang F, Gao S, Wang A, Fang W, Jin J. Zwitterionic nanohydrogel grafted PVDF membranes with comprehensive antifouling property and superior cycle stability for oil-in-water emulsion separation. *Adv Funct Mater*. **2018**;*28*:1804121.
27. Zhu Z, Wang W, Qi D, Luo Y, Liu Y, Xu Y, Cui F, Wang C, Chen X. Calcinable polymer membrane with revivability for efficient oily-water remediation. *Adv Mater*. **2018**;*30*:1801870.
28. Yin ZZ, Yuan F, Zhou DP, Xue MS, Luo YD, Hong Z, Xie C. Ultra dynamic water repellency and anti-icing performance of superhydrophobic ZnO surface on the printed circuit board (PCB). *Chem Phys Lett*. **2021**;*771*: 138558.
29. Yin ZZ, Yuan F, Xue MS, Xue YH, Xie Y, Ou JF, Luo YD, Hong Z, Xie C. A multifunctional and environmentally safe superhydrophobic membrane with superior oil/water separation, photocatalytic degradation and anti-biofouling performance. *J Colloid Interface Sci*. **2022**;*611*:93.
30. Cheng XQ, Jiao Y, Sun Z, Yang X, Cheng Z, Bai Q, Zhang Y, Wang K, Shao L. Constructing scalable superhydrophobic membranes for ultrafast water-oil separation. *ACS Nano*. **2021**;*15*:3500.
31. Yin ZZ, Xue MS, Luo YD, Hong Z, Xie C, Ren ZM, Wang H. Excellent static and dynamic anti-icing properties of hierarchical structured ZnO superhydrophobic surface on Cu substrates. *Chem Phys Lett*. **2020**;*755*: 137806.
32. Wang WW, Lin JX, Cheng JQ, Cui ZX, Si JH, Wang QT, Peng XF, Turng LS. Dual super-amphiphilic modified cellulose acetate nanofiber membranes with highly efficient oil/water separation and excellent antifouling properties. *J Hazard Mater*. **2020**;*385*: 121582.
33. Zhan YQ, He SJ, Wan XY, Zhao SM, Bai YL. Thermally and chemically stable poly(arylene ether nitrile)/halloysite nanotubes intercalated graphene oxide nanofibrous composite membranes for highly efficient oil/water emulsion separation in harsh environment. *J Membr Sci*. **2018**;*567*:76.
34. Chen XX, Yin ZZ, Yan JL, Xue MS, Chen YH, Yang CG, Luo YD. Fabrication of ZnO@Fe_2O_3 superhydrophobic coatings with high thermal conductivity. *Surf Coat Technol*. **2023**;*467*: 129701.
35. Deng YT, Xu FL, Yin ZZ, Xue MS, Chen YH, He P, Wu JS, Ou JF, Wang FJ, Luo YD, Hong Z. Controllable fabrication of superhydrophobic alloys surface on 304 stainless steel substrate for anti-icing performance. *Ceram Int*. **2023**;*49*:25135.
36. Chen X, Yin Z, Deng Y, Li Z, Xue M, Chen Y, Xie Y, Liu W, He P, Luo Y, Hong Z, Xie C. Harsh environment-tolerant and robust superhydrophobic graphene-based composite membrane for wearable strain sensor. *Sens Actuator A Phys*. **2023**;*362*: 114630.
37. Li M, Liu W, Yin Z, Yang H, Chen Y, Yang C, Luo Y, Hong Z, Xie C, Xue M. Facile fabrication of superhydrophobic and photocatalytic self-cleaning flexible strain sensor membrane for human motion. *Sens Actuator A Phys*. **2023**;*363*: 114750.
38. Wu JX, Zhang J, Kang YL, Wu G, Chen SC, Wang YZ. Reusable and recyclable superhydrophilic electrospun nanofibrous membranes with in situ co-cross-linked polymer-chitin nanowhisker network for robust oil-in-water emulsion separation. *Acs Sustain Chem Eng*. **2018**;*6*:1753.
39. Zhang LS, Fan W, Liu TX. Flexible hierarchical membranes of WS2 nanosheets grown on graphene-wrapped electrospun carbon nanofibers as advanced anodes for highly reversible lithium storage. *Nanoscale*. **2016**;*8*:16387.
40. Liu JH, Zhang C, Guo SH, Xu L, Xiao SJ, Shen ZG. Microwave treatment of pre-oxidized fibers for improving their structure and mechanical-properties. *Ceram Int*. **2019**;*45*:1379.
41. Tian D, Chen SH, Zhu WD, Wang C, Lu XF. Metal-organic framework derived hierarchical Ni/Ni3S2 decorated carbon nanofibers for high-performance supercapacitors. *Mater Chem Front*. **2019**;*3*:1653.
42. Ye W, Sun QL, Zhang GY. Effect of heat treatment conditions on properties of carbon-fiber-based electromagnetic-wave-absorbing composites. *Ceram Int*. **2019**;*45*:5093.
43. Zheng YW, Zhao W, Jia DD, Cui L, Liu JQ. Thermally-treated and acid-etched carbon fiber cloth based on pre-oxidized polyacrylonitrile as self-standing and high area-capacitance electrodes for flexible supercapacitors. *Chem Eng J*. **2019**;*364*:70.
44. Mao Q, Rajabpour S, Kowalik M, van Duin ACT. Predicting cost-effective carbon fiber precursors: Unraveling the functionalities of oxygen and nitrogen-containing groups during carbonization from ReaxFF simulations. *Carbon*. **2020**;*159*:25.
45. Sun SC, Cao WY. Evolution of microstructure within carbon fiber during pre-carbonization revealed by mean field theory. *Compos Commun*. **2022**;*34*: 101272.
46. Krishnamoorthi R, Anbazhagan R, Tsai H-C, Wang C-F, Lai J-Y. Biodegradable, superwettable caffeic acid/chitosan polymer coated cotton fibers for the simultaneous removal of oils, dyes, and metal ions from water. *Chem Eng J*. **2022**;*427*: 131920.
47. Xiao SJ, Cao WY, Wang B, Xu LH, Chen BH. Mechanism and kinetics of oxidation during the thermal stabilization of polyacrylonitrile fibers. *J Appl Polym Sci*. **2013**;*127*:3198.
48. Liu Y, Xue Y, Ji H, Liu J. Kinetics of the cyclization and isomerization reactions in polyacrylonitrile based carbon fiber precursors during thermal-oxidative stabilization. *J Appl Polym Sci*. **2020**;*137*:48819.
49. Karki HP, Kafle L, Ojha DP, Song JH, Kim HJ. Three-dimensional nanoporous polyacrylonitrile-based carbon scaffold for effective separation of oil from oil/water emulsion. *Polymer*. **2018**;*153*:597.
50. Pan H, Yang J, Wang S, Xiong Z, Cai W, Liu J. Facile fabrication of porous carbon nanofibers by electrospun PAN/dimethyl sulfone for capacitive deionization. *J Mater Chem A*. **2015**;*3*:13827.

51. Ma YX, Wan JY, Yang YF, Ye YS, Xiao X, Boyle DT, Burke W, Huang ZJ, Chen H, Cui Y, Yu ZA, Oyakhire ST. Scalable, ultrathin, and high-temperature-resistant solid polymer electrolytes for energy-dense lithium metal batteries. *Adv Energy Mater*. **2022**;*12*:2103720.
52. Sun X-L, Liu Z, Cheng Z-L. Design and fabrication of in-situ N-doped paper-like carbon nanofiber film for thiophene removal from a liquid model fuel. *J Hazard Mater*. **2020**;*389*: 121879.
53. Piper DM, Yersak TA, Son S-B, Kim SC, Kang CS, Oh KH, Ban C, Dillon AC, Lee S-H. Conformal Coatings of cyclized-PAN for mechanically resilient si nano-composite anodes. *Adv Energy Mater*. **2013**;*3*:697.
54. Wu M, Wang Q, Li K, Wu Y, Liu H. Optimization of stabilization conditions for electrospun polyacrylonitrile nanofibers. *Polym Degrad Stab*. **2012**;*97*:1511.
55. Kang HJ, Cheng ZJ, Lai H, Ma HX, Liu YY, Mai XM, Wang YS, Shao Q, Xiang LC, Guo XK, Guo ZH. Superlyophobic anticorrosive and self-cleaning titania robust mesh membrane with enhanced oil/water separation. *Sep Purif Technol*. **2018**;*201*:193.
56. Chen FZ, Lu Y, Liu X, Song JL, He GJ, Tiwari MK, Carmalt CJ, Parkin IP. Table salt as a template to prepare reusable porous PVDF-MWCNT foam for separation of immiscible oils/organic solvents and corrosive aqueous solutions. *Adv Funct Mater*. **2017**;*27*:1702926.
57. Li J, Kang RM, Tang XH, She HD, Yang YX, Zha F. Superhydrophobic meshes that can repel hot water and strong corrosive liquids used for efficient gravity-driven oil/water separation. *Nanoscale*. **2016**;*8*:7638.
58. Zhang ES, Cheng ZJ, Lv T, Qian YH, Liu YY. Anti-corrosive hierarchical structured copper mesh film with superhydrophilicity and underwater low adhesive superoleophobicity for highly efficient oil-water separation. *J Mater Chem A*. **2015**;*3*:13411.
59. Hayase G, Kanamori K, Fukuchi M, Kaji H, Nakanishi K. Facile synthesis of marshmallow-like macroporous gels usable under harsh conditions for the separation of oil and water. *Angew Chem Int Ed*. **1986**;*2013*:52.
60. Li Z, Zhang TC, Mokoba T, Yuan S. Superwetting Bi_2MoO_6/$Cu_3(PO_4)_2$ nanosheet-coated copper mesh with superior anti-oil-fouling and photo-fenton-like catalytic properties for effective oil-in-water emulsion separation. *Acs Appl Mater Interfaces*. **2021**;*13*:23662.
61. Modi A, Jiang Z, Kasher R. Hydrostable ZIF-8 layer on polyacrylonitrile membrane for efficient treatment of oilfield produced water. *Chem Eng J*. **2022**;*434*: 133513.
62. Chen S, Liu Y, Wang Y, Xu K, Zhang X, Zhong W, Luo G, Xing M. Dual-functional superwettable nano-structured membrane: from ultra-effective separation of oil-water emulsion to seawater desalination. *Chem Eng J*. **2021**;*411*: 128042.
63. Zhang N, Yang N, Zhang L, Jiang B, Sun Y, Ma J, Cheng K, Peng F. Facile hydrophilic modification of PVDF membrane with Ag/EGCG decorated micro/nanostructural surface for efficient oil-in-water emulsion separation. *Chem Eng J*. **2020**;*402*: 126200.
64. Yang C, Wang Z, Long M, Qin B, Wang Y, Zhi K, Zheng Y, Zhao J, Li W, Wang Z, Zhang M, Zhang R, Wu H, Jiang Z. Antifouling poly(phenylene sulfide) membrane with an amphiphilic surface for efficient oil/water separation. *J Membr Sci*. **2023**;*679*: 121690.
65. Wang Y, Yang H, Yang Y, Zhu L, Zeng Z, Liu S, Li Y, Liang Z. Poly(vinylidene fluoride) membranes with underwater superoleophobicity for highly efficient separation of oil-in-water emulsions in resisting fouling. *Sep Purif Technol*. **2022**;*285*: 120298.
66. Zhu YZ, Xie W, Zhang F, Xing TL, Jin J. Superhydrophilic in-situ-cross-linked zwitterionic polyelectrolyte/PVDF-blend membrane for highly efficient oil/water emulsion separation. *Acs Appl Mater Interfaces*. **2017**;*9*:9603.
67. Zhang LY, He Y, Luo PY, Ma L, Fan Y, Zhang SH, Shi H, Li SS, Nie YL. A heterostructured PPy/ZnO layer assembled on a PAN nanofibrous membrane with robust visible-light-induced self-cleaning properties for highly efficient water purification with fast separation flux. *J Mater Chem A*. **2020**;*8*:4483.
68. Zhang LY, He Y, Ma L, Chen JY, Fan Y, Zhang SH, Shi H, Li ZY, Luo PY. Hierarchically stabilized PAN/β-FeOOH nanofibrous membrane for efficient water purification with excellent antifouling performance and robust solvent resistance. *Acs Appl Mater Interfaces*. **2019**;*11*:34487.
69. Jing J, Yin R, Yuan Y, Shi Y, Sun J, Zhang M. Determination of the transportation limits of heavy crude oil using three combined methods of heating, water blending, and dilution. *ACS Omega*. **2020**;*5*:9870.
70. Mason TJ. Ultrasonic cleaning: an historical perspective. *Ultras Sonochem*. **2016**;*29*:519.